Elsevier Editorial System(tm) for Scripta Materialia

Manuscript Draft

Manuscript Number: SMM-16-330R1

Title: Mechanical properties of Bi2Te3 topological insulator investigated by density functional theory and nanoindentation

Article Type: Regular article

Keywords: nanoindentation; Young's modulus; thermoelectric materials; topological insulators; density functional theory

Corresponding Author: Dr. Antonio Politano,

Corresponding Author's Institution: Università degli Studi della Calabria

First Author: Caterina Lamuta

Order of Authors: Caterina Lamuta; Davide Campi; Anna Cupolillo; Mahammad B Babanly; Evgueni V Chulkov; Antonio Politano; Leonardo Pagnotta

Abstract: The elastic constants Cij of bulk Bi2Te3 were calculated by density functional theory by different approximations. Computational results were validated by means of nanoindentation tests, performed along the directions parallel and perpendicular to the cleavage plane of Bi2Te3. The indentation modulus was estimated and compared with the experimental one. The generalized gradient Perdew-Burke-Ernzerhof approximation better reproduces experimental results in the direction perpendicular to the cleavage plane, whereas the occurrence of the nanobuckling in the direction parallel to the cleavage plane causes discrepancies between theoretical and experimental findings.

*Graphical Abstract

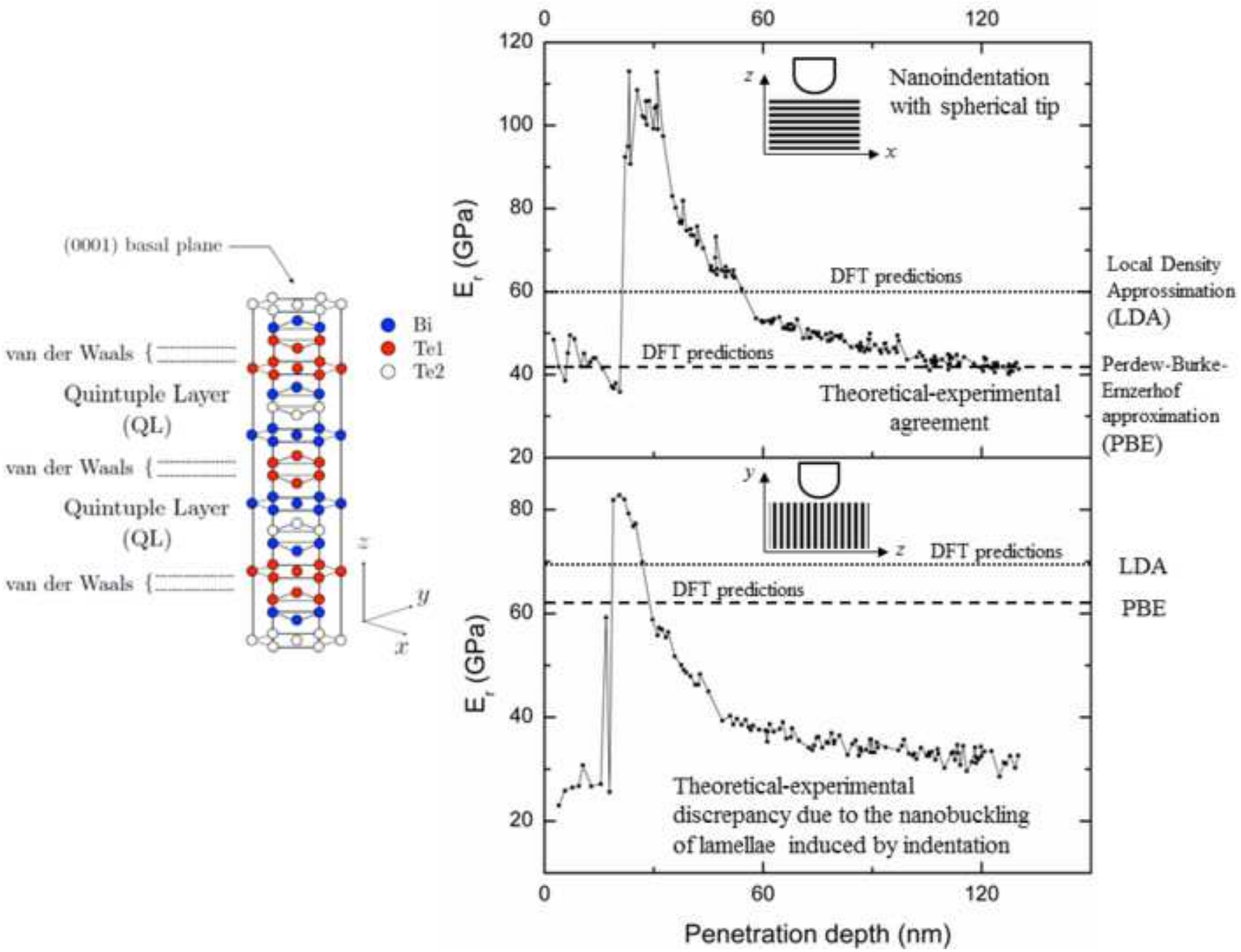

Cover Letter

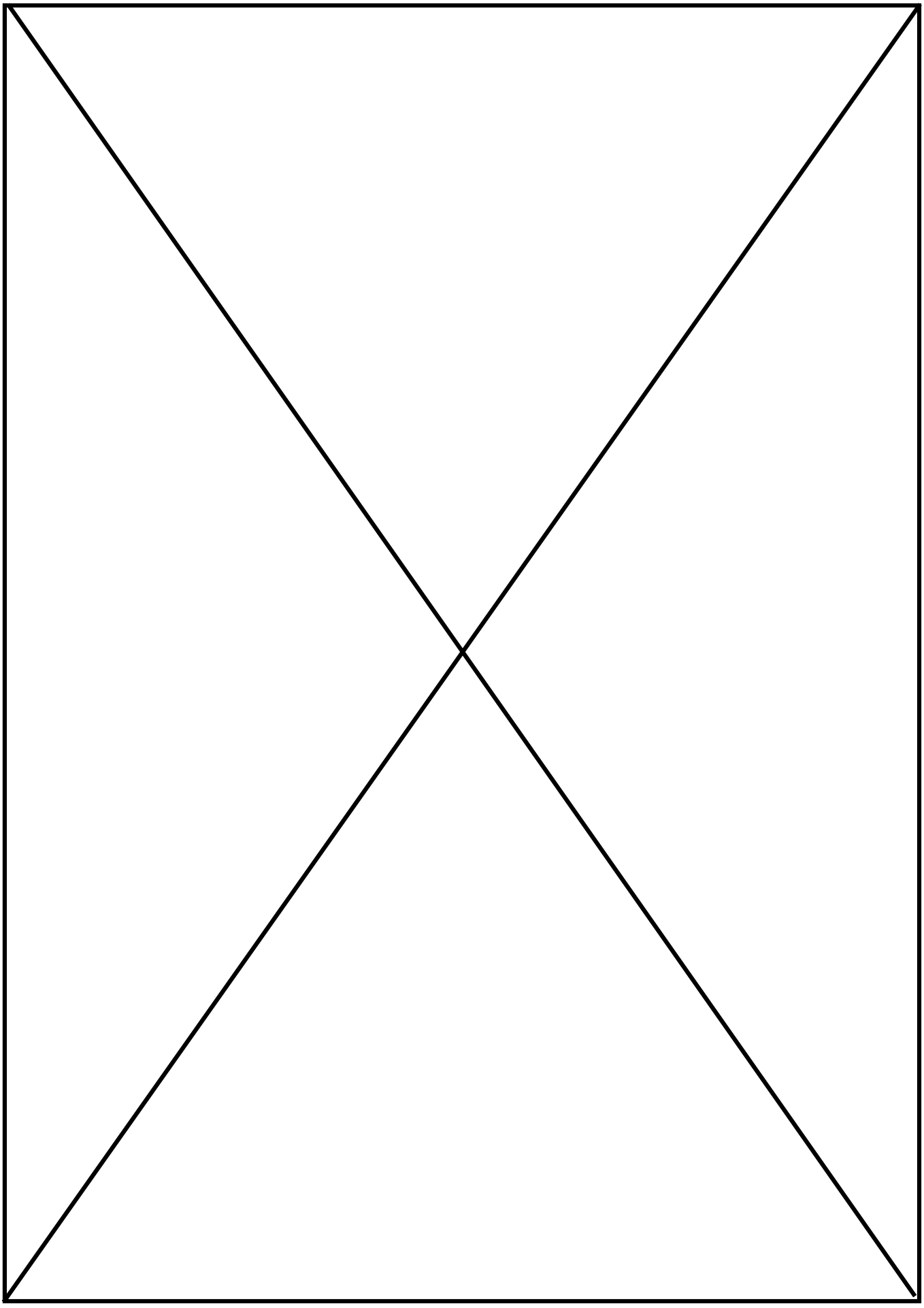

***Response to Reviewers**

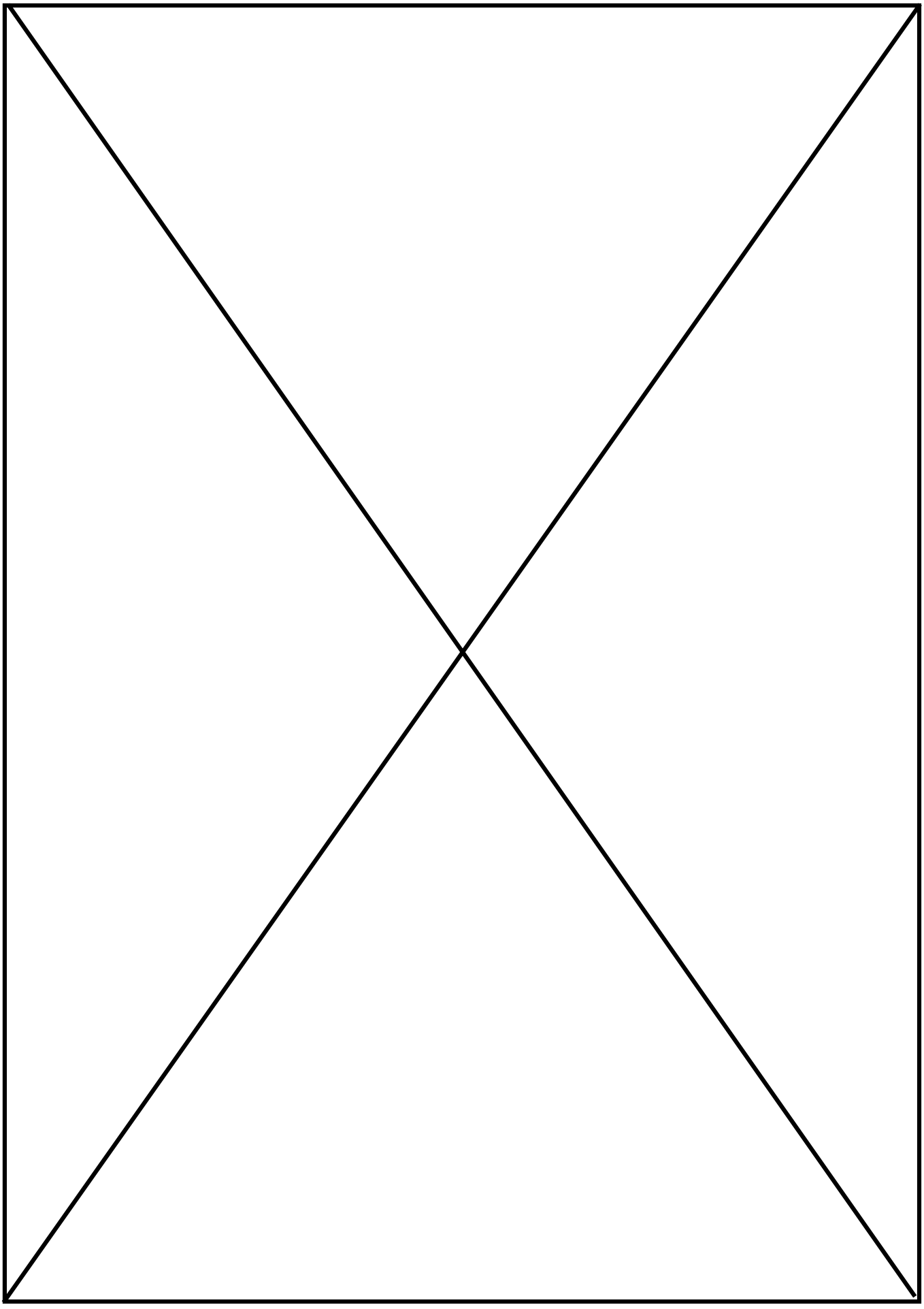

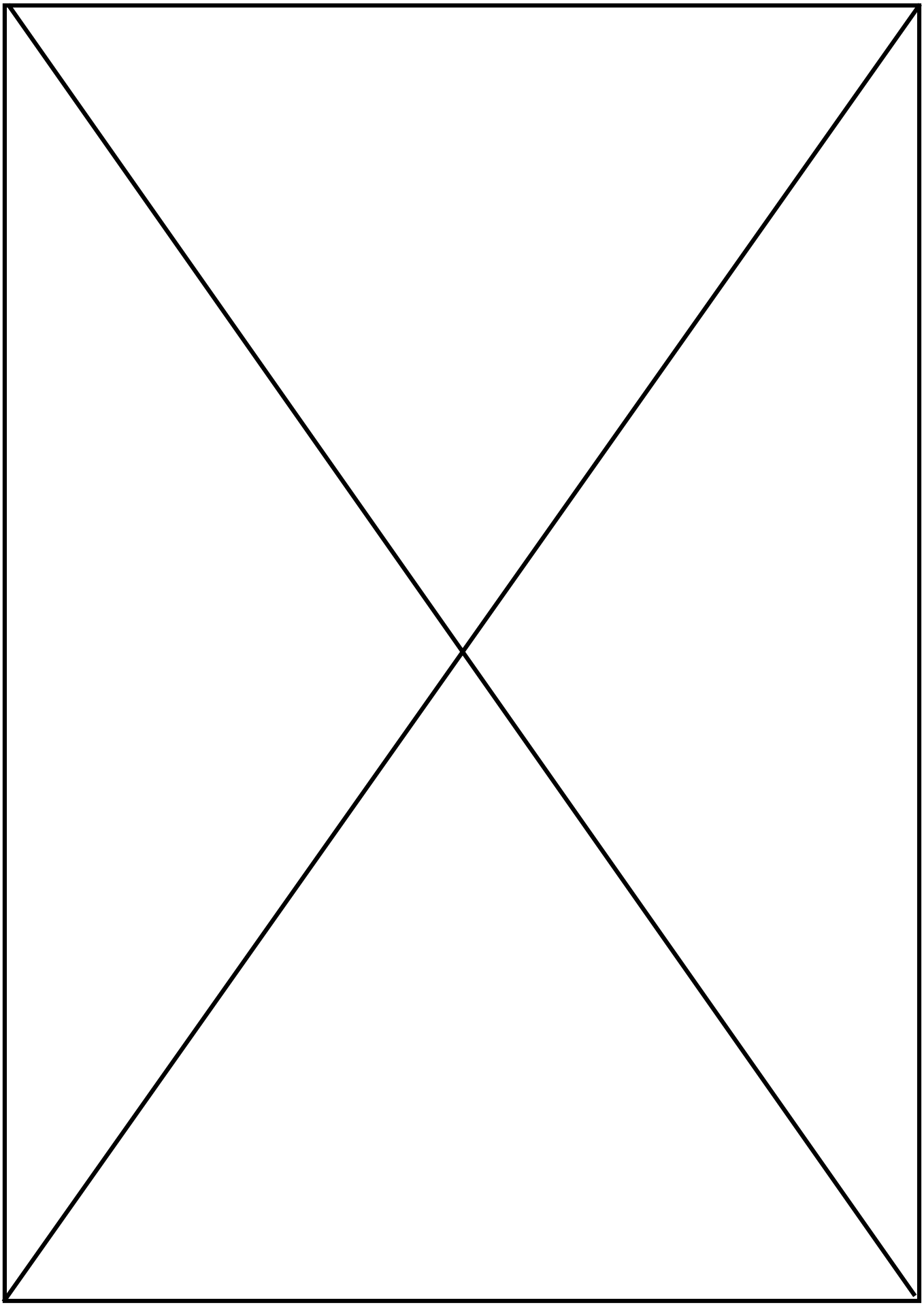

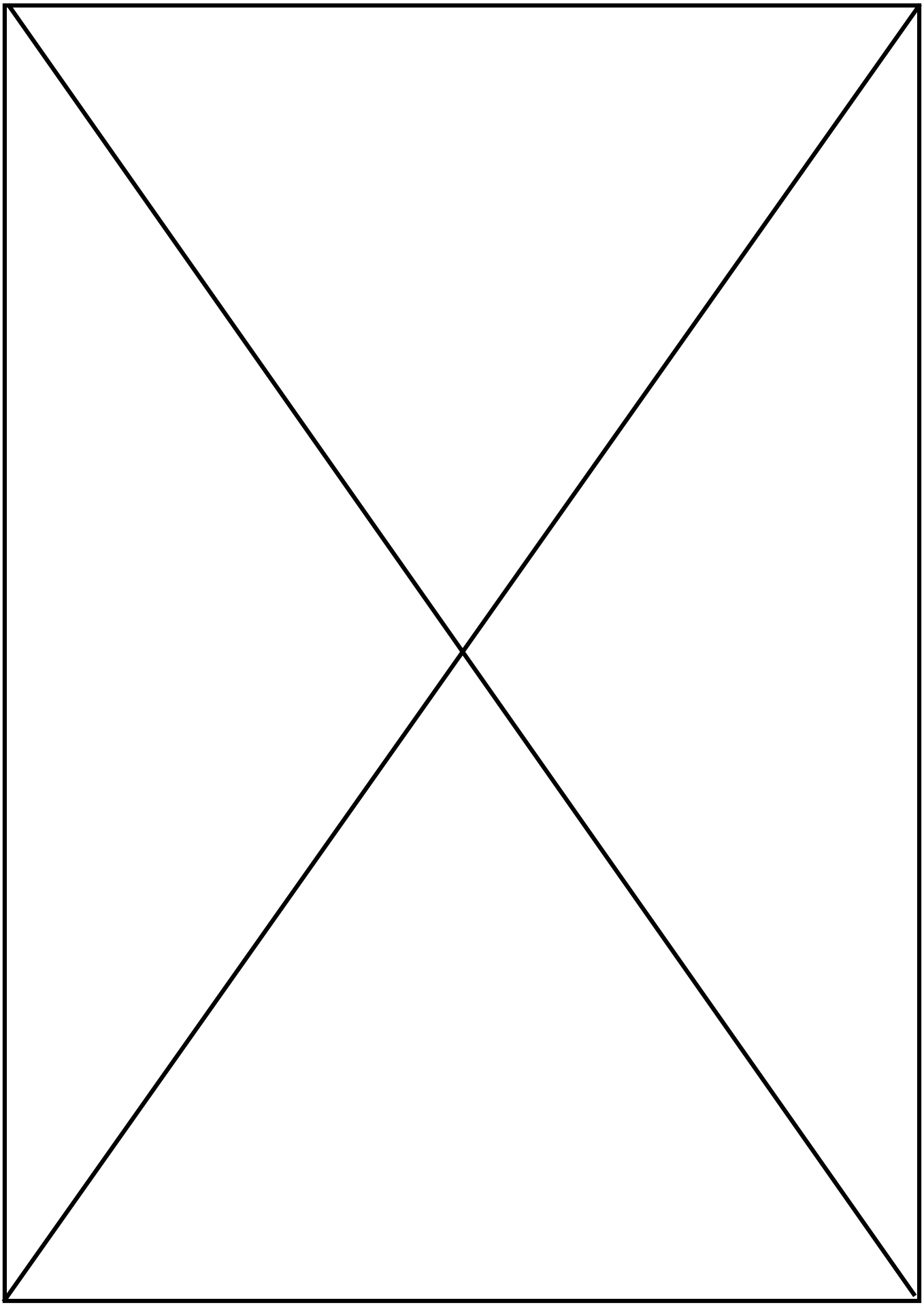

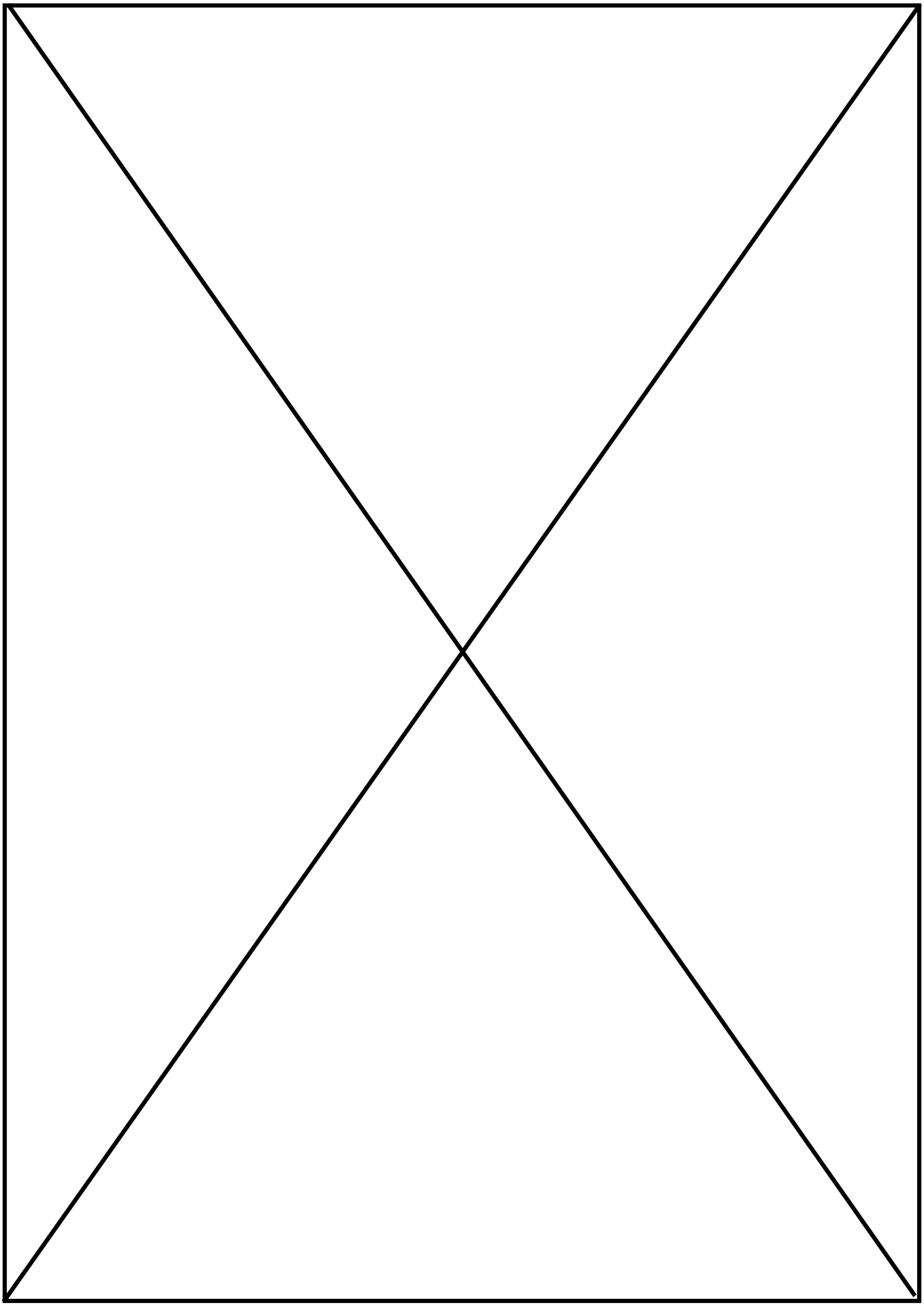

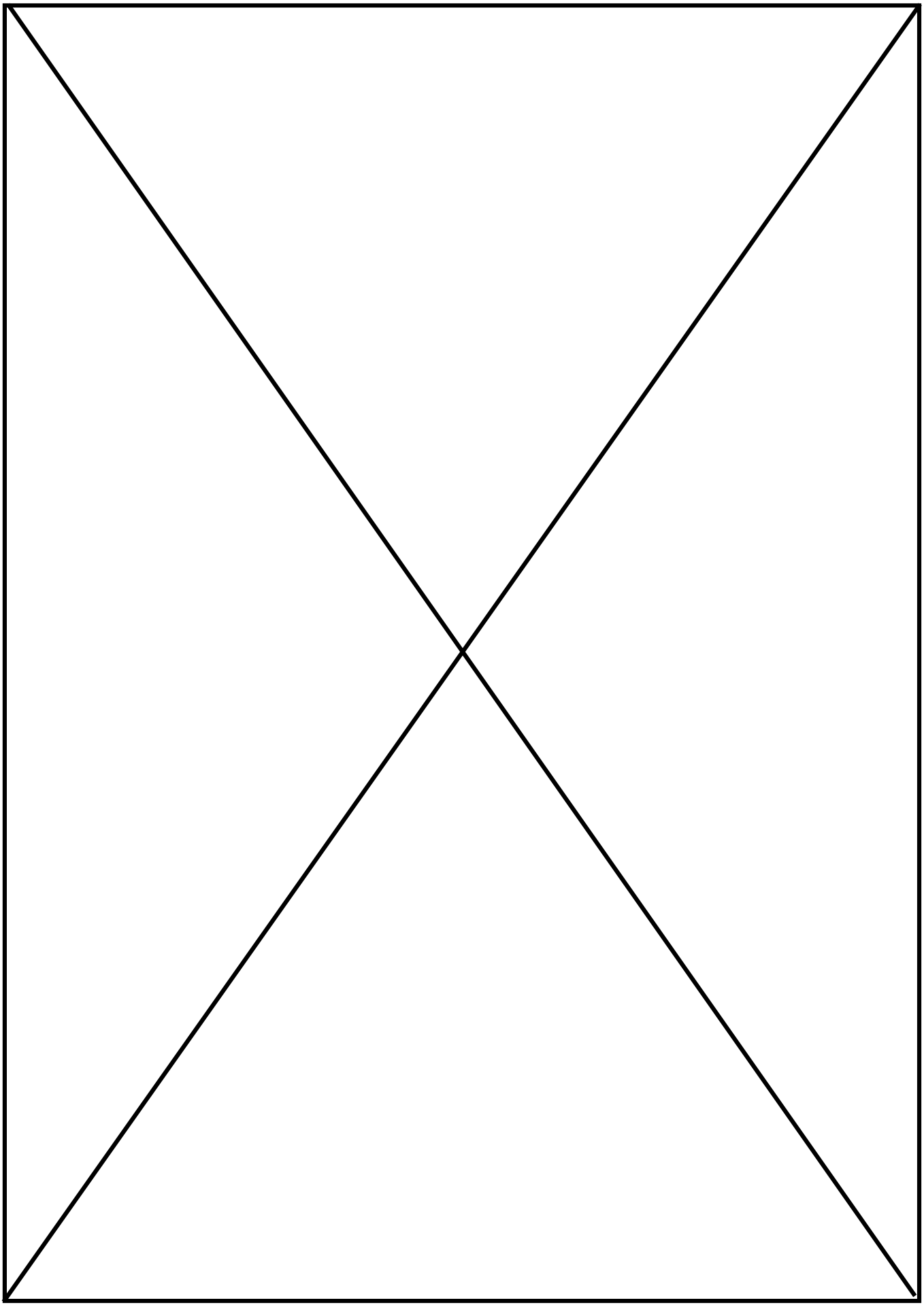

Mechanical properties of Bi_2Te_3 topological insulator investigated by density functional theory and nanoindentation

C. Lamuta[a,*], D. Campi[b], A. Cupolillo[c], Z. S. Aliev[d,e,f], M. B. Babanly[e], E. V. Chulkov[d,g,h,i,j], A. Politano[c,*], L. Pagnotta[a]

[a]*Department of Mechanical, Energy and Management Engineering, University of Calabria, Ponte P. Bucci, Cubo 44C, 87036 Rende, Italy*

[b] *Department of Materials Science, University of Milano-Bicocca, via R. Cozzi 55, I-20125, Milano, Italy*

[c]*Department of Physics, University of Calabria, Ponte P. Bucci, Cubo 31C, 87036 Rende, Italy*

[d] *Donostia International Physics Center (DIPC), Paseo de Manuel Lardizabal 4, 20018 San Sebastián/Donostia, Spain*

[e] *Institute of Catalysis and Inorganic Chemistry, ANAS, AZ1143 Baku, Azerbaijian*

[j] *Institute of Physics, ANAS, AZ1143 Baku, Azerbaijian*

[g] *Departamento de Fisica de Materiales, Universidad del Pais Vasco, Apartado 1072, 20080 San Sebastián/Donostia, Spain*

[h]*Centro de Fisica de Materiales CFM-Materials Physics Center MPC, Centro Mixto CSIC-UPV/EHU, Paseo de Manuel Lardizabal 5, 20018 San Sebastián/Donostia, Spain*

[i]*Saint Petersburg State University, 198504 Saint Petersburg, Russian*

[j]*Tomsk State University, 634050 Tomsk, Russian Federation*

Abstract

The elastic constants C_{ij} of bulk Bi_2Te_3 were calculated by density functional theory by different approximations. Computational results were validated by means of nanoindentation tests, performed along the directions parallel and perpendicular to the cleavage plane of Bi_2Te_3. The indentation modulus was estimated and compared with the experimental one. The generalized gradient Perdew-Burke-Ernzerhof approximation better reproduces experimental results in the direction perpendicular to the cleavage plane, whereas the occurrence of the nanobuckling in the direction parallel to the cleavage plane causes discrepancies between theoretical and experimental findings.

*corresponding authors

Caterina Lamuta (caterinalamuta@gmail.com) & Antonio Politano (antonio.politano@fis.unical.it)

1. Introduction

Novel topological phases of matter, such as 3D topological insulators (TIs), are having huge impact in fundamental research [1-3]. TIs have vast application capabilities in optoelectronics [4], plasmonics [5], spintronics [6], quantum computing [7], and for thermoelectric devices [2, 8, 9]. Among TIs, bismuth chalcogenides such as Bi_2Te_3 and Bi_2Se_3 are suitable for applications at room temperature, due to their large energy gap (~0.2-0.3 eV), and, therefore, they have been widely investigated [10, 11]. However, to date mainly basic research has been carried out on TIs. Despite the wealth of experimental works, the number of patents based on TI technology is hitherto scarce, mainly as a consequence of issues related to the crystalline quality of most TI samples. The presence of vacancies shifts the position of the Fermi level, altering the properties of the TI system [12]. Thus, in most cases, the Fermi level is shifted from the bulk band gap and pinned by the bulk states occupied by doping electrons or holes. TI samples with vacancies cannot be successfully used in technology, since the surface conductivity due to the topological surface states is overshadowed by contributions from the topologically trivial bulk conduction band. Moreover, the presence of vacancies favors the formation of Bi-O bonds [13], thus inducing the rapid oxidation [14-16] and, consequently, the degradation of the surface of TIs. The optimized use of the Bridgman-Stockbarger method in vacuum/inert atmosphere can strongly reduce the amount of vacancies in TI samples [17]. This implies chemical inertness toward surface oxidation [17-19]. Moreover, such a notable control on growth methods allows tuning the position of the Fermi level [20] or even the position of the Dirac point [21], thus paving the way for band-structure engineering of TI heterostructures [22]. Therefore, TIs are now ripe to move ahead, beyond basic research. Raw TI materials could be engineered to be used in innovative applications in several areas, as recently demonstrated for TI-based Terahertz photodetectors [23].

The study of mechanical properties is crucial for designing many technological applications as nanoelectromechanical systems (NEMS) [24, 25] and flexible electronic devices [26] and, moreover, for the promising prospect of TI-based mechanical metamaterials [27]. However, the comprehension of mechanical properties of TIs is still unsatisfactory.

Bi_2Te_3 is an anisotropic layered material, with a R-3m symmetry, and it is characterized by six independent elastic moduli. Such moduli were firstly measured by Jenkins at al. using a continuous-wave resonance technique [28]. Afterwards, several computational studies, employing both classical interatomic potential models and ab-initio calculations, were carried out in order to predict the thermo-mechanical properties of bulk bismuth telluride along different directions [29-31]. Concerning experimental characterizations, with the aim to probe hardness and Young's modulus, indentation tests were performed on Bi_2Te_3 thin films [32], suspended few-layer flakes [33] and, recently, on the bulk material grown with the Bridgman-Stockbarger method [34].

However, all these indentation investigations disregarded the anisotropic behavior of bismuth chalcogenides since the tests were carried out only in the direction perpendicular to the (0001) basal plane. It is important to notice that, to date, mechanical properties of bismuth chalcogenides have been evaluated within the framework of the model by Oliver and Pharr [35, 36], which has been developed for isotropic materials. A more careful treatment of nanoindentation data is required in order to properly describe the anisotropic mechanical properties of bismuth chalcogenides.

Herein, we report a joint experimental and theoretical investigation of mechanical properties of bulk single crystals of Bi_2Te_3 by taking into account the material anisotropy. In particular, depth sensing nanoindentation tests were carried out along two different directions, parallel and perpendicular to the basal plane, in order to measure the indentation Young's modulus. Density functional theory (DFT) calculations, with different exchange-correlation functional approximations, were performed in order to obtain the stiffness matrix of Bi_2Te_3 and, subsequently, a theoretical estimate of the indentation modulus by using the model developed in Ref. [37].

An overall good agreement between experimental and theoretical results was found. The obtained results were also compared with those of the literature in order to provide a clear outline on the mechanical properties of Bi_2Te_3.

2. Methods

2.1 Sample growth and characterization

A single crystalline ingot of Bi_2Te_3 was grown from melt by the vertical Bridgman−Stockbarger method in the conical-bottom quartz ampoule sealed under a vacuum. In the growth process, the ampoule moves from the "hot" zone (80 K higher than melting point) to the "cold" zone with the required rate of 1.2 mm/h. The temperature of the "cold" zone was about 100 K lower than the melting point. The grown ingot consisted of one or several large single crystalline blocks ,which show chemical inertness toward surface oxidation for even one month in air, as shown elsewhere [18]. Fresh surfaces were readily available by cleaving the crystals along their natural cleavage plane, to obtain (0001)-oriented surfaces.

The specimens were then carefully cut, cleaved and glued on a sample-holder, in both parallel and perpendicular directions with respect to the natural cleavage plane, in order to be tested by nanoindentation.

Sample crystallinity was assessed through X-Ray Diffraction (XRD) analyses, whereas the absence of any contaminant in the topmost layers of the surface was verified by X-ray photoelectron spectroscopy (XPS), as shown elsewhere [34]. By analyzing core levels in XPS spectra [18], the absence of surface oxide phases even after having exposed samples to large doses of oxygen or even after air exposure can be claimed. As a matter of fact, the amount of defects in single-crystal samples used in this investigation is minimized so that the oxidation rate, driven just by surface defects [13], is negligible even after months in air, contrarily to previous reports for bismuth chalcogenides [14, 38].

2.2 Computational details

Bi_2Te_3 has an rhombohedral crystal structure with five atoms per unit cell. It belongs to the D^5_{3d} (R-3m) space group. The structure consists of covalently bonded quintuple layers [Se(1)-Bi-Se(2)-Bi-Se(1)] separated by weak Van der Waals bonds (Figure 1).

The structural and elastic properties of Bi_2Te_3 were calculated using DFT, as implemented in the QUANTUM-ESPRESSO package [39], using a norm conserving scalar relativistic pseudopotentials with only the outermost *s* and *p* states in valence band. Both the local density approximation (LDA) [40] and the generalized gradient Perdew-Burke-Ernzerhof (PBE) [41] approximation for the exchange-correlation energy functional were used. A semiempirical Van der Waals correction, as described in Ref. [42], was added in the case of PBE approximation. The electronic wave functions were expanded in plane waves up to a 90 Ry energy cut-off. We optimized the bulk geometry using the non-elemental hexagonal cell and by integrating the Brillouin zone over a 8x8x2 Monkhorst-Pack mesh [43]. Atomic positions were relaxed until the forces were below a $5 \cdot 10^{-5}$ a.u. threshold. The lattice parameters for the optimized geometries are reported in Table 1 compared with the experimental values.

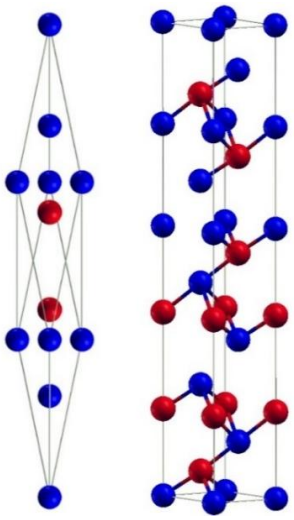

Figure 1: Unit cell (rhombohedral) and conventional cell (hexagonal) of Bi_2Te_3. Bismuth atoms are represented in red, tellurium atoms in blue.

Table 1: equilibrium lattice parameters

	Experimental values	**LDA**	**PBE+VDW**
Lattice parameters [Å]	a=4.38 c=30.50	a=4.33 c=29.82	a=4.31 c=30.94

The obtained values of equilibrium lattice parameters for both LDA and PBE+VDW are in good agreement with experimental values [44] within an error of 1.1% and 1.5% in the two cases, respectively, and, moreover, with previous ab-initio calculations [45].

The elastic constants were evaluated from the stress-strain relation, following the procedure described in Refs. [46, 47] and applying deformations from 0.2% to 2%.

2.3 Model for the estimation of the indentation modulus for anisotropic materials

Depth-sensing indentation is a useful and powerful tool for mechanical characterization of materials at micro- and nano- scale. This technique allows determining the Young's modulus and the material hardness from the analysis of the load-displacement curves according to the Oliver and Pharr's theory [30, 31]. Concerning Young's modulus, such theory estimates the reduced Young's modulus E_r, also called indentation modulus M, by means of formula (1):

$$E_r = M = \frac{S\sqrt{\pi}}{2\sqrt{A(h_c)}} \quad (1)$$

where S is the slope of the unloading curve at maximum displacement and $A(h_c)$ is an estimate of the contact area between tip and material as a function of the effective penetration depth h_c. Oliver

and Pharr modeled the unloading process by the contact of a paraboloid of revolution on a half space, giving h_c as:

$$h_c = h_{max} - \varepsilon \frac{P_{max}}{S_{max}} \quad (2)$$

where h_{max} is the maximum penetration depth, P_{max} is the maximum indentation load, S_{max} the slope of the unloading curve at the maximum load and ε is equal to 3/4. The Young's modulus of the indented material can be calculated by formula (3):

$$E = \frac{(1-\nu^2)}{\frac{1}{E_r} - \frac{(1-\nu_i{}^2)}{E_i}} \quad (3)$$

where ν is the material Poisson's ratio, whereas E_i and ν_i are the Young's modulus and the Poisson's ratio of the indenter material (typically E_i = 1141 GPa and ν_i = 0.07 for a diamond tip).

However, equations (1), (2) and (3) are related to homogeneous and isotropic materials and they have to be modified when an anisotropic material is analyzed by means of indentation tests.

Vlassak and Nix [48] studied the contact problem of a flat circular punch and a paraboloid on an elastically anisotropic half space and they showed that Equations (1) and (2) can be used for anisotropic materials as long as the half space has three of fourfold rotational symmetry. In the case of lower symmetry, the indentation modulus depends on the shape of the indenter. Subsequently, they proposed [49] a relation in order to estimate the indentation modulus E_r from the stiffness matrix of an arbitrary anisotropic solid (alternative to Equation (3)). However, such a relation is a really complex and it can be analytically solved only in particular cases, such as for transversely isotropic materials [50]. Recently, Vlassak et al [37] simplified relation of Ref. [49] and suggested a simple equation for the estimation of the indentation modulus:

$$M = \frac{1}{\pi h_0} \quad (4)$$

where h_0 is the first term of the Fourier series expansion of surface Green's function and it can be obtained from the elastic constants C_{ij} of the anisotropic material. Model in Ref. [35] was generalized for indenters of arbitrary shapes and verified on different anisotropic materials, also on

solids with a R-3m symmetry, like Bi_2Te_3 single crystal analyzed in this work. For these reasons, we chose this model in order to estimate the theoretical indentation modulus of bulk Bi_2Te_3 by using C_{ij} constants calculated by DFT. The estimated modulus was then compared with the experimental one, obtained by means of nanoindentation tests.

The constant h_0 is also related to the angle between the tip's axis and the material basal plane. Our decision to indent along the directions parallel and perpendicular to the Bi_2Te_3 basal plane is motivated by the easiness of sample preparation for indentation tests.

2.4 Indentation tests

Nanoindentation tests were performed on Anton Paar Nano Indenter provided with a spherical tip (R = 20μm, α = 90°) and the mechanical properties, i.e. hardness (H) and the reduced Young's modulus (E_r), were determined in the directions perpendicular and parallel to the (0001) basal plane.

In particular, the Continuous Stiffness Measurements (CSM) technique [42] was deployed. It consists in superimposing a small-amplitude oscillation on the force signal and it allows recording the reduced Young's modulus, E_r, and the hardness, H, dynamically, for increasing values of the penetration depth.

For the direction parallel to the basal plane the following indentation parameters were set: amplitude of the sinusoidal varying force 0.5 mN, frequency 20 Hz, maximum load 5 mN, loading rate 5 mN/min, unloading rate 20 mN/min, holding time at maximum load 10 s.

For the direction perpendicular to the basal plane the following parameters were used: amplitude of the sinusoidal varying force 1 mN, frequency 20 Hz, maximum load 10 mN, loading rate 10 mN/min, unloading rate 40 mN/min, holding time at maximum load 10 s.

A dynamic calibration of the nanoindenter was carried out before testing, whereas the distance between each indents was kept at least three times the maximum diagonal of the imprint in order to avoid the mutual influence of adjacent indentations.

The mechanical properties were obtained according to the Oliver and Pharr theory [30, 31]. In particular, the experimental indentation modulus was obtained according to Equation (1).

3. Results and discussion

Bulk Bi_2Te_3 is a layered anisotropic material and, thus, it is characterized by different mechanical properties along different directions.

DFT calculations, with the parameters described in section 2.2, were carried out in order to put in evidence the anisotropic behavior of mechanical properties. In table 2, the six independent coefficients of the stiffness matrix of Bi_2Te_3, obtained with both the LDA approximation and the PBE approximation with the semiempirical Van der Waals correction (PBE+VDW), are reported and compared with data available in literature.

Table 2: Comparison of calculated and experimental elastic modulus C_{ij}

	C_{11}	C_{12}	C_{13}	C_{14}	C_{33}	C_{44}
LDA (our work)	81.5	22.2	31.2	19.4	56.4	42.7
PBE-VDW (our work)	78.3	13.8	23.2	20.7	35.7	35.5
Experiment Ref. [28]	74.4	21.7	27.0	13.3	47.7	27.4
DFT, Ref. [51]	65.4	14.0	19.0	10.9	50.7	26.5

The analysis of data in Table 2 indicates that LDA well reproduces the experimental values of C_{12} and C_{13}, while PBE-VDW better reproduces C_{11}. On the other hand, the theoretical model in Ref. [51] is appropriate for reproducing C_{14}, C_{44} and C_{66} and it also fails for C_{11}, C_{12}, and C_{13}.

The corresponding indentation moduli, along directions parallel and perpendicular to the c axis of the hexagonal cell, calculated according to Equation (4) by using C_{ij} constants in Table 2, are reported in Table 3.

Table 3: Comparison of calculated indentation moduli

	Perpendicular to the lamellae (GPa)	Parallel to the lamellae (GPa)
LDA (our work)	60.21	69.45
PBE-VDW (our work)	42.46	62.40
Experiment Ref. [28]	47.71	59.74
DFT, Ref. [51]	51.26	57.67

To experimentally validate computational results, nanoindentation test were carried out (according to methodologies listed in Section 2.4).

In Figure 2 the trend of the reduced Young's modulus E_r as a function of the penetration depth is shown for both the indentation directions, perpendicular (top panel) and parallel (bottom panel) to the cleavage plane. One can observe that for the direction perpendicular to the cleavage plane, when E_r stabilizes, it reaches exactly the value of the indentation modulus calculated using the PBE+VDW approximation. The value of the indentation modulus estimated with the LDA approximation is instead considerably higher than the experimental one. This can be ascribed to the problem of over-binding usually shown by the LDA approximation that lead to higher binding

energies and shorter bond lengths with respect to the experimental ones and that becomes particularly relevant in presence of weak Van der Waals bonds.

As shown in Figure 2, the indentation moduli estimated by using data reported in literature lie in the middle of the range defined by our LDA and PBE+VDW calculations.

Along the direction parallel to cleavage plane (bottom panel) all calculated values of E_r are rather higher than the experimental value after data stabilization.

In order to explain these differences along the two directions of indentation, in the following we provide some considerations about the effect of the indentation process on layered materials. Different studies on the indentation of layered material were carried out [52-54]. In particular, it was observed that along the direction perpendicular to the cleavage plane the formation of kink bands can occur [53]. Kink bands are walls of dislocations of opposed polarity, which develop on the indented material after the contact with the tip. They cause the delamination of material's layers. Such a delamination can be observed on the indented sample as a surface bulging around the indentation area and it mainly occurs with sharp tips and high indentation loads, as observed in Ref. [34]. This damage can be also observed in the load-penetration depth curve, characterized by pop-in phenomena [34].

For this work, as described in Section 2.4, indentation tests were performed with a spherical tip at very low loads by using the CSM technique in order to avoid the material damage during the indentation process, which could lead to a misleading estimation of mechanical properties. Any damage was indeed observed on the indented samples, as well as any pop-in phenomena was recorded in the load-penetration depth curves. Indentation experimental results can thus be compared to computational ones.

It is worth reminding that previous studies carried out on pyrolytic carbon [52, 54] along the direction parallel to the cleavage plane showed the occurrence of elastic nanobuckling of the material layers also for low indentation loads. Thus, the discrepancies observed in the bottom panel

of Figure 2 between theoretical and experimental results can be related to the nanobuckling induced during the indentation process, which leads to an underestimation of mechanical properties.

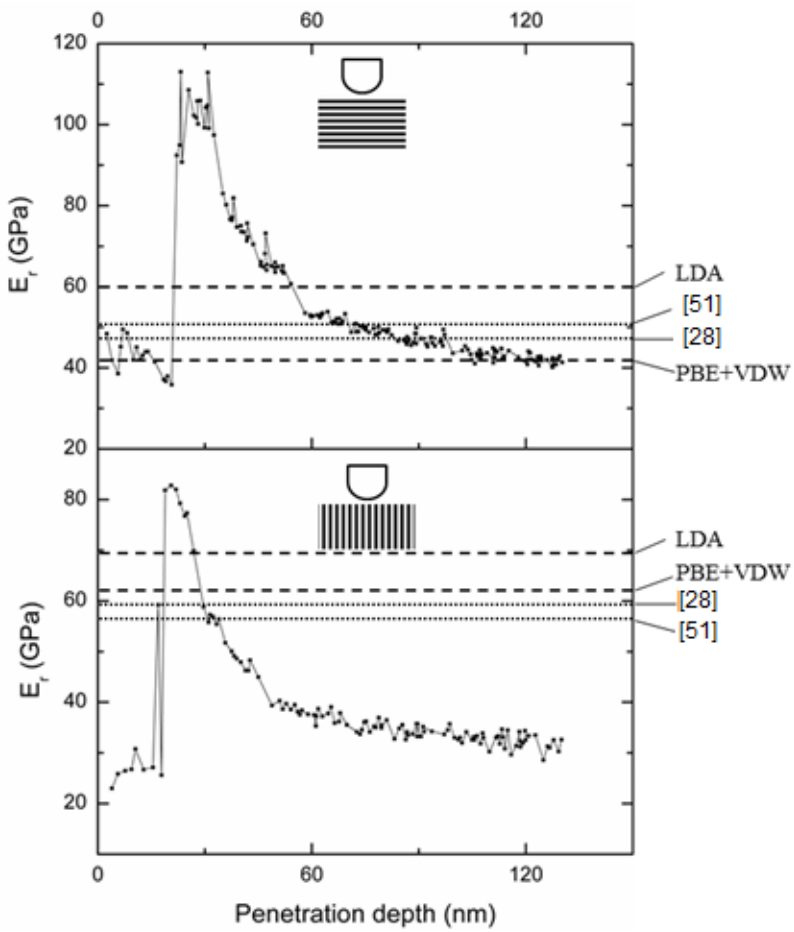

Figure 2: E_r profile with increasing values of penetration depth for a CSM nanoindentation carried out along the direction perpendicular (top panel) and parallel (bottom panel) to the cleavage plane. The dashed lines represent the indentation modulus calculated according to Equation (4) using constants C_{ij} calculated with the LDA and PBE+VDW approximations, whereas the dotted lines refer to constants C_{ij} reported in literature.

Also the measured value of hardness is lower in the direction parallel to the cleavage plane (Figure 3). For the perpendicular direction (top panel), the hardness stabilizes around 1.7 GPa whereas its saturation value is about 0.9 GPa in the parallel direction (bottom panel). As observed for the

Bi_2Te_3 thin films [55], the hardness has an initial increase at small penetration depth, attributed to the transition between purely elastic to elastic/plastic contact, and a following decrease until a stabilized value, related to the transition between elastic/plastic and fully plastic contacts. Until the fully plastic contact is not reached, the measured hardness is actually reflecting the mean contact pressure and it does not represent the intrinsic hardness of the material.

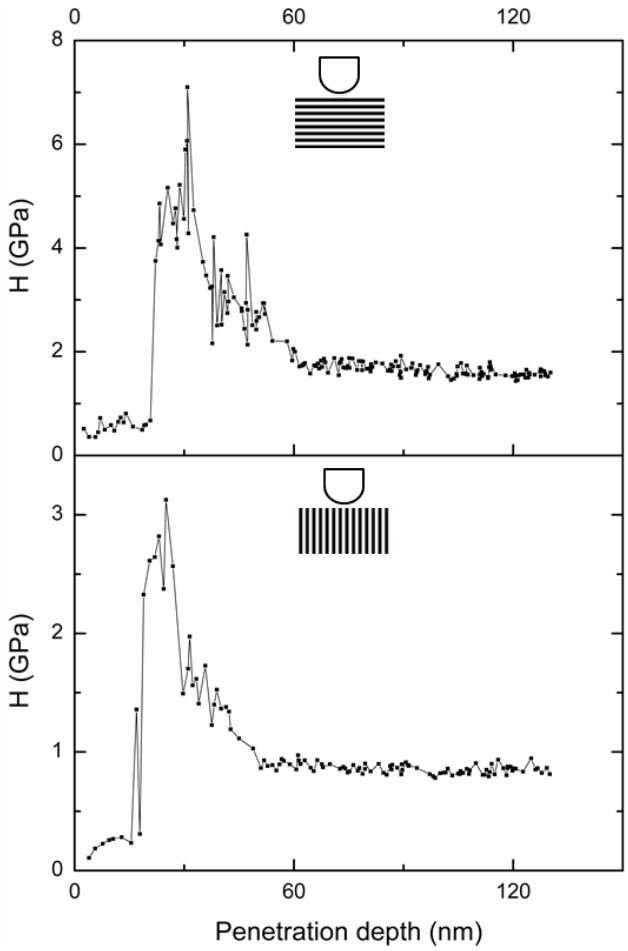

Figure 3: H profile with increasing values of penetration depth for a CSM nanoindentation carried out along the direction perpendicular (top panel) and parallel (bottom panel) to the cleavage plane.

4. Conclusions

By means of DFT and nanoindentation tests, we have studied the mechanical properties of bismuth telluride by taking into account its anisotropy. While tip-induced nanoscale buckling affects the measurement of the indentation Young's modulus along the cleavage plane (predicted to be 62.40 GPa by DFT but experimentally found to be ~38 GPa by nanoindentation), the experimental value of the indentation Young's modulus in the perpendicular direction with respect to the cleavage plane is well reproduced by DFT using PBE-VDW (42.46 GPa). PBE-VDW better reproduces experimental results with respect to LDA.

Present work ─ combining state-of-the-art growth of TI single crystals, nanoindentation, and DFT calculations ─ significantly improves the comprehension of mechanical properties of TIs, thus paving the way toward their control at the nanoscale for technological applications.

Acknowledgments

The authors thank prof. M. Ciaravella for helpful discussions on mechanical properties in anisotropic materials.

Authors acknowledge MaTeRiA project (Grant No. PONa3_00370) for providing equipment to perform nanoindentation experiments.

EVC acknowledge funding from the University of Basque Country UPV/EHU (GIC07-IT-756-13), the Departamento de Educación del Gobierno Vasco and the Spanish Ministerio de Ciencia e Innovación (FIS2010-275 19609-C02-01), the Tomsk State University Academic D.I. Mendeleev Fund Program (Grant No.8.1.05.2015), the Spanish Ministry of Economy and Competitiveness MINECO (Grant No. FIS2013-48286-C2-1-P), and Saint Petersburg State University (Project No. 11.50.202.2015)

References

[1] C. Wang, A.C. Potter, T. Senthil, Science 343 (2014) 629-631.

[2] O. Caballero-Calero, M. Martín-González, Scr. Mater. 111 (2016) 54-57.

[3] J. Jacimovic, X. Mettan, A. Pisoni, R. Gaal, S. Katrych, L. Demko, A. Akrap, L. Forro, H. Berger, P. Bugnon, A. Magrez, Scr. Mater. 76 (2014) 69-72.

[4] H. Peng, W. Dang, J. Cao, Y. Chen, D. Wu, W. Zheng, H. Li, Z.X. Shen, Z. Liu, Nature Chem. 4 (2012) 281-286.

[5] I.A. Nechaev, I. Aguilera, V. De Renzi, A. di Bona, A. Lodi Rizzini, A.M. Mio, G. Nicotra, A. Politano, S. Scalese, Z.S. Aliev, M.B. Babanly, C. Friedrich, S. Blügel, E.V. Chulkov, Phys. Rev. B 91 (2015) 245123.

[6] I. Vobornik, U. Manju, J. Fujii, F. Borgatti, P. Torelli, D. Krizmancic, Y.S. Hor, R.J. Cava, G. Panaccione, Nano Lett. 11 (2011) 4079-4082.
[7] C. Nayak, S.H. Simon, A. Stern, M. Freedman, S. Das Sarma, Rev. Mod. Phys. 80 (2008) 1083-1159.
[8] D. Li, X.Y. Qin, Y.C. Dou, X.Y. Li, R.R. Sun, Q.Q. Wang, L.L. Li, H.X. Xin, N. Wang, N.N. Wang, C.J. Song, Y.F. Liu, J. Zhang, Scr. Mater. 67 (2012) 161-164.
[9] Y. Liu, M. Zhou, J. He, Scr. Mater. 111 (2016) 39-43.
[10] J.L. Zhang, S.J. Zhang, H.M. Weng, W. Zhang, L.X. Yang, Q.Q. Liu, S.M. Feng, X.C. Wang, R.C. Yu, L.Z. Cao, L. Wang, W.G. Yang, H.Z. Liu, W.Y. Zhao, S.C. Zhang, X. Dai, Z. Fang, C.Q. Jin, Proc. Natl. Acad. Sci., U. S. A. 108 (2011) 24-28.
[11] H. Yuan, H. Liu, H. Shimotani, H. Guo, M. Chen, Q. Xue, Y. Iwasa, Nano Lett. 11 (2011) 2601-2605.
[12] T.R. Devidas, E.P. Amaladass, S. Shilpam, R. Rajaraman, D. Sornadurai, N. Subramanian, M. Awadhesh, C.S. Sundar, A. Bharathi, Europhys. Lett. 108 (2014) 67008.
[13] V.A. Golyashov, K.A. Kokh, S.V. Makarenko, K.N. Romanyuk, I.P. Prosvirin, A.V. Kalinkin, O.E. Tereshchenko, A.S. Kozhukhov, D.V. Sheglov, S.V. Eremeev, S.D. Borisova, E.V. Chulkov, J. Appl. Phys. 112 (2012) 113702.
[14] D. Kong, J.J. Cha, K. Lai, H. Peng, J.G. Analytis, S. Meister, Y. Chen, H.J. Zhang, I.R. Fisher, Z.X. Shen, Y. Cui, ACS Nano 5 (2011) 4698-4703.
[15] J.H. Hwang, S. Kwon, J. Park, J.H. Kim, J. Lee, J.S. Kim, H.-K. Lyeo, J.Y. Park, Appl. Phys. Lett. 104 (2014) 161613.
[16] J.H. Hwang, J. Park, S. Kwon, J.S. Kim, J.Y. Park, Surf. Sci. 630 (2014) 153-157.
[17] V.V. Atuchin, V.A. Golyashov, K.A. Kokh, I.V. Korolkov, A.S. Kozhukhov, V.N. Kruchinin, S.V. Makarenko, L.D. Pokrovsky, I.P. Prosvirin, K.N. Romanyuk, O.E. Tereshchenko, Cryst. Growth Des. 11 (2011) 5507-5514.
[18] A. Politano, M. Caputo, S. Nappini, F. Bondino, E. Magnano, Z.S. Aliev, M.B. Babanly, A. Goldoni, G. Chiarello, E.V. Chulkov, J. Phys. Chem. C 118 (2014) 21517–21522.
[19] L.V. Yashina, J. Sánchez-Barriga, M.R. Scholz, A.A. Volykhov, A.P. Sirotina, V.S. Neudachina, M.E. Tamm, A. Varykhalov, D. Marchenko, G. Springholz, G. Bauer, A. Knop-Gericke, O. Rader, ACS Nano 7 (2013) 5181-5191.
[20] P. Wei, Z. Wang, X. Liu, V. Aji, J. Shi, Phys. Rev. B 85 (2012) 201402.
[21] S. Roy, H.L. Meyerheim, A. Ernst, K. Mohseni, C. Tusche, M.G. Vergniory, T.V. Menshchikova, M.M. Otrokov, A.G. Ryabishchenkova, Z.S. Aliev, M.B. Babanly, K.A. Kokh, O.E. Tereshchenko, E.V. Chulkov, J. Schneider, J. Kirschner, Phys. Rev. Lett. 113 (2014) 116802.
[22] T.V. Menshchikova, M.M. Otrokov, S.S. Tsirkin, D.A. Samorokov, V.V. Bebneva, A. Ernst, V.M. Kuznetsov, E.V. Chulkov, Nano Lett. 13 (2013) 6064-6069.
[23] L. Viti, D. Coquillat, A. Politano, K.A. Kokh, Z.S. Aliev, M.B. Babanly, O.E. Tereshchenko, W. Knap, E.V. Chulkov, M.S. Vitiello, Nano Lett. 16 (2016) 80–87.
[24] S.J. Cartamil-Bueno, P.G. Steeneken, F.D. Tichelaar, E. Navarro-Moratalla, W.J. Venstra, R. Leeuwen, E. Coronado, H.S.J. Zant, G.A. Steele, A. Castellanos-Gomez, Nano Res. 8 (2015) 2842-2849.
[25] A. Politano, G. Chiarello, Nano Res. 8 (2015) 1847-1856.
[26] W. Zhu, M.N. Yogeesh, S. Yang, S.H. Aldave, J.-S. Kim, S. Sonde, L. Tao, N. Lu, D. Akinwande, Nano Lett. 15 (2015) 1883-1890.
[27] R. Süsstrunk, S.D. Huber, Science 349 (2015) 47-50.
[28] J.O. Jenkins, J.A. Rayne, R.W. Ure, Phys. Rev. B 5 (1972) 3171-3184.
[29] S. Feng, S. Li, H. Fu, Comp. Mater. Sci. 82 (2014) 45-49.
[30] Y. Tong, F. Yi, L. Liu, P. Zhai, Q. Zhang, Comp. Mater. Sci. 48 (2010) 343-348.
[31] Z. Xiong, X. An, Z. Li, T. Xiao, X. Chen, J. Alloys Compd. 586 (2014) 392-398.
[32] C.-H. Tasi, Y.-C. Tseng, S.-R. Jian, Y.-Y. Liao, C.-M. Lin, P.-F. Yang, D.-L. Chen, H.-J. Chen, C.-W. Luo, J.-Y. Juang, J. Alloys Compd. 619 (2015) 834-838.
[33] L. Guo, H. Yan, Q. Moore, M. Buettner, J. Song, L. Li, P.T. Araujo, H.-T. Wang, Nanoscale 7 (2015) 11915-11921.
[34] C. Lamuta, A. Cupolillo, A. Politano, Z.S. Aliev, M.B. Babanly, E.V. Chulkov, L. Pagnotta, Nano Res. (2016) doi:10.1007/s12274-12016-10995-z.
[35] W.C. Oliver, G.M. Pharr, J. Mater. Res. 7 (1992) 1564-1583.

[36] W.C. Oliver, G.M. Pharr, J. Mater. Res. 19 (2004) 3-20.
[37] J.J. Vlassak, M. Ciavarella, J.R. Barber, X. Wang, J. Mech. Phys. Solids 51 (2003) 1701-1721.
[38] H. Bando, K. Koizumi, Y. Oikawa, K. Daikohara, V.A. Kulbachinskii, H. Ozaki, J. Phys.: Condens. Matter 12 (2000) 5607.
[39] P. Giannozzi, S. Baroni, N. Bonini, M. Calandra, R. Car, C. Cavazzoni, D. Ceresoli, G.L. Chiarotti, M. Cococcioni, I. Dabo, A. Dal Corso, S. de Gironcoli, S. Fabris, G. Fratesi, R. Gebauer, U. Gerstmann, C. Gougoussis, A. Kokalj, L. Michele, L. Martin-Samos, N. Marzari, F. Mauri, R. Mazzarello, S. Paolini, A. Pasquarello, L. Paulatto, C. Sbraccia, S. Scandolo, G. Sclauzero, A.P. Seitsonen, A. Smogunov, P. Umari, R.M. Wentzcovitch, J. Phys.: Condens. Matter 21 (2009) 395502.
[40] J.P. Perdew, A. Zunger, Phys. Rev. B 23 (1981) 5048-5079.
[41] J.P. Perdew, K. Burke, M. Ernzerhof, Phys. Rev. Lett. 77 (1996) 3865-3868.
[42] S. Grimme, J. Comput. Chem. 27 (2006) 1787-1799.
[43] H.J. Monkhorst, J.D. Pack, Phys. Rev. B 13 (1976) 5188-5192.
[44] R.W.G. Wyckoff, Crystal Structures, Wiley and Sons, New York, 1964.
[45] V. Chis, I.Y. Sklyadneva, K.A. Kokh, V.A. Volodin, O.E. Tereshchenko, E.V. Chulkov, Phys. Rev. B 86 (2012) 174304.
[46] P.T. Jochym, K. Parlinski, M. Sternik, Eur. Phys. J. B 10 9-13.
[47] P.T. Jochym, K. Parlinski, Eur. Phys. J. B 15 265-268.
[48] J.J. Vlassak, W.D. Nix, Philos. Mag. A 67 (1993) 1045-1056.
[49] J.J. Vlassak, W.D. Nix, J. Mech. Phys. Solids 42 (1994) 1223-1245.
[50] J.R. Willis, J. Mech. Phys. Solids 14 (1966) 163-176.
[51] B.-L. Huang, M. Kaviany, Phys. Rev. B 77 (2008) 125209.
[52] T.S. Gross, N. Timoshchuk, I.I. Tsukrov, R. Piat, B. Reznik, ZAMM Z. Angew. Math. Mech. 93 (2013) 301-312.
[53] M.W. Barsoum, A. Murugaiah, S.R. Kalidindi, T. Zhen, Y. Gogotsi, Carbon 42 (2004) 1435-1445.
[54] T.S. Gross, N. Timoshchuk, I. Tsukrov, B. Reznik, Carbon 60 (2013) 273-279.
[55] S.-R. Jian, C.-H. Tasi, S.-Y. Huang, C.-W. Luo, J. Alloys Compd. 622 (2015) 601-605.